RSC Advances

PAPER

View Article Online
View Journal | View Issue

Cite this: *RSC Adv.*, 2024, **14**, 38746

Electrospinning of methacrylated alginate for tissue engineering applications

Daria Poshina,*[a] Natalia Sokolova,[a] Steve Nono-Tagne,[b] Hamed Ahmadi-Nohadani,[b] Iosif Gofman,[a] Alexander Mishanin,[c] Alexey Golovkin,[c] Yury Skorik[ac] and Issei Otsuka *[b]

Photo-crosslinkable methacrylated alginate derivatives (M-ALGs) were synthesized *via* modification of sodium alginate with glycidyl methacrylate. Needle (capillary) and needleless electrospinning techniques were employed to produce their nonwoven fiber mats. Spinning parameters such as applied voltage, solution composition, and flow rate were optimized to form uniform bead-free fibers with an average diameter of about 150 nm. The needleless technique allowed successful electrospinning of M-ALG solutions with wider ranges of viscosities and surface tensions owing to its higher applicable voltage (~65 kV) compared to that of the needle technique (~30 kV). Photo-crosslinking of the fibers *via* UV irradiation allowed the fiber mats to remain insoluble in physiological media while maintaining their mechanical properties. Cultivation of multipotent mesenchymal stem cells (MSCs) with the cross-linked fiber mats in a modified Eagle medium (α-MEM) showed the growth of spherical colonies, indicating the sufficient cytocompatibility of the fiber mats with MSCs.

Received 22nd October 2024
Accepted 21st November 2024

DOI: 10.1039/d4ra07559e

rsc.li/rsc-advances

Introduction

Natural polysaccharides have great potential for use as biomedical materials because of their biocompatibility, biodegradability, and hydrophilicity. Notably, their electrospun fibrous mats provide a supportive environment for cellular growth owing to their high porosity and resemblance to the natural extracellular matrix (ECM).[1,2] The high porosity of electrospun scaffolds can promote tissue regeneration through the intensive exchange of media and metabolites. Electrospun scaffolds exhibit a porosity of 93–95%[3] by volume and can provide effective swelling, fluid retention, and excessive fluid drainage when used as wound dressings. Functional groups in polysaccharides can be chemically modified, allowing fine tuning of their properties according to application targets. Polysaccharides have been widely used for biomedical applications and as scaffolds for wound healing and cell culture. In particular, alginic acid, which is an abundantly available water-soluble polysaccharide derived from sea algae, has attracted intensive attention owing to its unique biological activity. Alginic acid consists of irregularly alternating β-D-mannuronic acid and α-L-guluronic acid residues linked by a (1 → 4)-glycosidic linkage.[4] Alginate (ALG), which is a salt form (typically with sodium) of alginic acid mainly found in algal cell walls, has been widely used in the food industry and medicine considering its exceptional biocompatibility, biodegradability, gelling properties, and low cost.[5] These properties make ALG a promising material for drug-delivery systems, wound dressings, and scaffolds for cell culture.[3]

Alginate is characterized as non-degradable in mammals because of the absence of alginases. Although alginate gels can be dissolved in mammalian physiological media, alginate molecules cannot be completely eliminated from the body on account of the high average molecular weight of commercially available alginates.[6] Thus, for *in vivo* use, it is important to use alginate with a molecular weight below 50 kDa, which is the size threshold for efficient renal clearance.[7] Partial oxidation of alginate chains can make alginate degradable under physiological conditions.[8] However, alginate is still promising in topical tissue regeneration application, such as wound dressings.

The main drawbacks of electrospun polysaccharide scaffolds are their water solubility and poor mechanical properties. Various physical and chemical crosslinking methods have been developed to overcome these drawbacks.[9] Recently, photochemical crosslinking has attracted much interest as a fast, efficient, solvent-free, and easily controllable method. It also allows preserving the as-spun fiber mat structures, in contrast with other methods such as ion gelation and wet spinning techniques.[10] Photo-crosslinkable polysaccharides have also been successfully applied in preparations of hydrogels.[11] Photo-

[a]*Institute of Macromolecular Compounds, Branch of Petersburg Nuclear Physics Institute named by B.P. Konstantinov, National Research Centre Kurchatov Institute, Bolshoy pr. V.O. 31, 199004 St Petersburg, Russia. E-mail: poschin@yandex.ru*

[b]*Univ. Grenoble Alpes, CNRS, CERMAV, Grenoble 38000, France. E-mail: issei.otsuka@cermav.cnrs.fr*

[c]*Almazov National Medical Research Centre, Akkuratova str. 2., 197341 St. Petersburg, Russia*

crosslinking helps to fix the structure of the hydrogels, which increases their mechanical properties, reduces their solubilities, and allows an easy entrapment of cells and growth factors within the hydrogels used as tissue engineering scaffolds.[12] In many cases, methacrylate groups have been used as photo-crosslinkable units. Commonly, ALG has been methacrylated by reaction with methacrylic anhydride,[13] glycidyl methacrylate (GM),[13,14] and 2-aminoethyl methacrylate.[13,15] For tissue engineering applications, the main factors affecting cell survival are the type of solvent, the duration of crosslinking, and the toxicity of the photo-initiator.[16] Photo-crosslinkable ALG containing low doses of initiator sufficient for crosslinking was shown to be non-toxic and also biodegradable.[15] Other hydrogels based on hyaluronic acid and collagen modified with methacrylic anhydride supported fibroblast adhesion and proliferation.[17]

The structure of the scaffold plays another important role in cell culture. The high porosity of electrospun fiber mats provides for the effective removal of cell metabolites, as well as good delivery of nutrients and oxygen. Nanofibers form numerous contacts with the cell membrane,[18] mimicking the cell microenvironment specifically close to the natural ECM.[19] Nowadays, electrospinning is considered to be one of the most straightforward and widespread techniques to obtain nano- or submicron fibers with diameters ranging from *ca.* 50 to 500 nm. In this technique, high electrical tension is applied to a polymer solution to generate liquid jets from the spinning electrode to form fibers *via* evaporation of the solvent during the jets' flight to the counter electrode.[20] The properties of the resulting fibers strongly depend on the solution composition, process parameters, and environmental conditions. Therefore, it is necessary to optimize these parameters for particular polymer and electrospinning methods. The main obstacle in the electrospinning of aqueous polysaccharide solutions is their high surface tension, which makes it difficult to form stable jets to maintain the electrospinning process.[21] Previously, this was overcome by co-electrospinning ALG with "carrier polymers", such as polyethylene oxide (PEO) and polyvinyl alcohol (PVA), in the presence of surfactants and salts.[22] However, there have been only a handful of studies on the electrospinning of photo-crosslinkable polysaccharides, *e.g.*, (i) sodium hyaluronate modified with 3-(2-furyl)acrylic acid,[23] α,β-unsaturated carboxylic acids,[23] and maleic anhydride,[24,25] (ii) chitosan (CS) modified with maleic anhydride,[26] ethylene glycol acrylate methacrylate,[27] and methacrylic anhydride,[28] and (iii) dextran modified with methacrylic anhydride.[29] Although ALG is one of the most promising polysaccharides for biomedical applications, to the best of our knowledge, only one study on the cytocompatibility of electrospun photo-crosslinkable ALG[30] has been reported to date. Therefore, further study on the electrospinning of photo-crosslinkable ALG and its fiber properties still needs to be investigated more thoroughly.

In this work, we used conventional needle (capillary) electrospinning and highly productive needleless electrospinning techniques to form nonwoven fiber mats from methacrylated ALG (M-ALGs) synthesized by the modification of sodium ALG with GM. The obtained fiber mats were photo-crosslinked *via* UV irradiation and their physical and biological properties, including morphology, mechanical strength, and cytocompatibility with multipotent mesenchymal stem cells (MSCs), were investigated toward their tissue engineering applications.

Experimental

Materials

Alginic acid sodium salt (viscosity; 15–25 cP (1% in H_2O)), GM (97%), PEO ($M_w = 4.0 \times 10^5$ Da), Triton X-100 surfactant (laboratory grade), deuterium oxide (99.9%), 2-hydroxy-4'–(2-hydroxyethoxy)-2-methylpropiophenone (I2959 : 98%), fetal bovine serum, modified Eagle medium (α-MEM), L-glutamine, penicillin-streptomycin, and phosphate buffered saline (PBS) were purchased from Sigma-Aldrich and used without further purification. CS ($M_w = 6.0 \times 10^4$ Da, degree of deacetylation of 0.82) was purchased from Bioprogress and used without further purification.

Instruments

NMR spectra were recorded with a Bruker Avance 400 MHz spectrometer. Fourier transform infrared (FTIR) spectra were recorded with a Bruker Vertex 70 spectrometer. Dynamic viscosity was measured with a Fungilab Viscolead Pro rotational viscometer. Surface tension was determined with a K20 Tensiometer (Kruss) using the Wilhelmy plate method. The conductivity of the solutions was recorded with a Hanna EC215 conductometer. The needle (capillary) electrospinning of the M-ALGs was carried out using a Fuence Esprayer ES-2000S2A machine using an 18 GA needle. The needleless electrospinning of M-ALGs was carried out using a NanoSpider NS Lab 500 machine. Scanning electron microscopy (SEM) images were obtained using a FEI Quanta 250 FEG SEM instrument at an accelerating voltage of 2.5 kV. Atomic force microscopy (AFM) images were obtained using an NT-MDT Zelenograd SMENA instrument in the tapping mode with a resonant frequency of 146 kHz and spring constant of 58 N m^{-1} using a cantilever with a 10 nm curvature tip. Fluorescence microscope images were obtained using a Carl Zeiss AxioObserver microscope. Tensile tests were performed using a Shimadzu AG-100kNX Plus universal mechanical testing system in the uniaxial tensile mode at room temperature.

Molecular characterization of ALG

The intrinsic viscosity of ALG ($[\eta] = 4.26$ dL g^{-1}) was determined using an Ubbelohde viscometer at 20 °C in 0.1 M NaCl. The viscosity average molecular weight of ALG ($M_\eta = 1.25 \times 10^5$ Da) was calculated using the Mark–Houwink–Sakurada equation: $[\eta] = 4.85 \times 10^{-3} \times M_\eta^{0.97}$.[31] The fraction of guluronate (G) units *vs.* mannuronate (M) units in ALG ($F_G = G\ (G^{-1} + M)$) was determined from the ^{1}H NMR spectrum of ALG according to the method reported by Grasdalen *et al.*[32]

Synthesis of methacrylated alginates (M-ALGs)

M-ALGs were synthesized as reported elsewhere.[13] A typical procedure for the synthesis of M-ALG having the degree of substitution (DS) of the methacrylate group of 0.55 is described

below. First, 2 g of sodium ALG was dissolved in 100 mL of distilled water. Acetic acid was added dropwise to the solution until pH became 3.5. Then, 5.5 mL of GM (molar ratio of ALG : GM = 1 : 4) was added to the solution under continuous stirring. The solution was stirred at 60 °C for 5.5 h with periodically adjusting the pH to 3.5 with acetic acid. The product was precipitated with ethanol, washed with tetrahydrofuran to remove residues of GM, then washed with ethanol followed by lyophilization from its aqueous solution to give M-ALG as a white solid.

Electrospinning

M-ALGs were dissolved in water to make 2–4% (w/v) solutions. PEO (10–50% by weight of M-ALGs) was added to the solutions as a carrier polymer. Triton X-100 (0.1–1% (w/v)) was then added to the mixtures in order to reduce their surface tension. Finally, the photoinitiator I2959 (0.3% (w/v)) was added to the mixtures followed by electrospinning. For the needle electrospinning, the applied voltage was kept at 30 kV, the distance between the needle and a grounded collector was kept at 15 cm, and the solution flow rate was varied from 2 to 30 μL min^{-1}. For the needleless electrospinning, the distance between the string electrode and a grounded collector was kept at 22 cm, the rotation speed of the spinning electrode was kept at 8 rpm, and the applied voltage was varied from 60 to 65 kV. For MSCs cultivation, two electrospun fiber mats were prepared. First, CS was electrospun from its 2% solution in acetic acid (50% aq.) with PEO (0.4% (w/v)) by the needleless process (60 kV, 22 cm between the electrodes, 8 rpm). The obtained CS fiber mat was heated at 80 °C under vacuum for 3 h to remove excessive acetic acid, and used as the control sample. Second, M-ALG was electrospun on the electrospun CS fiber mat by the needleless process using the optimized parameters described above. The CS/M-ALG double-layered fiber mat was first irradiated with UV light to crosslink M-ALG, and then heated at 80 °C under vacuum for 3 h to remove excessive acetic acid.

Photo-crosslinking

To ensure the photo-crosslinking ability of the M-ALGs (DS = 0.30 and 0.55), they were irradiated in the form of aqueous solutions (4% w/v) and electrospun fiber mats in the presence of photoinitiator I2959. UV irradiation was carried out for 30 min with an intensity of 200 mW cm^{-2} using a 312 nm UV-light source.

Morphology characterization

The average fiber diameters and pore sizes in the electrospun fiber mats were determined by analyzing the SEM images using ImageJ software. The average fiber diameters were calculated from 100 different fibers randomly selected from the images. The average pore sizes were determined by determining the areas of the pore marked in the image by hand. The average roughness of the fiber mat was determined by analyzing the AFM images using Gwyddion software as the difference between the lowest and the highest height-values in the set of 5 profiles in 5 images.

Mechanical property characterization

For the tensile test, the samples were cut into 40 × 4 mm strips and stretched at a rate of 10 mm min^{-1}. The Young's modulus (E), tensile strength (σ_y), breaking stress (σ_b), and elongation at break (ε_b) were determined from the stress–strain curve.

Cytocompatibility characterization *via* MSCs cultivation

MSCs were obtained from the subcutaneous adipose tissue of healthy male Wistar rats as described previously.[33] Briefly, fragments of adipose tissue were washed extensively, dissociated in 5 mg ml^{-1} collagenase III solution (Worthington Biochemical Corp., Lakewood, NJ, USA) and cultured as described below.

The cytocompatibility of the electrospun fiber mats was investigated according to a previously reported method.[3,34] Adipose-tissue-derived rat MSCs were cultured with the electrospun fiber mats in α-MEM medium supplemented with 10% fetal bovine serum, 1% L-glutamine, and 1% penicillin/streptomycin at 37 °C in a 5% CO_2 atmosphere. All the materials were additionally disinfected with 70% ethanol solution followed by three washes with PBS and exposure to α-MEM medium for 24 h. The medium was replaced then with fresh medium and the MSCs were added at a concentration of 5×10^4 cells/mL. After 72 h, the samples were washed with PBS and fixed with 4% paraformaldehyde for 10 min. Next, the MSCs were stained with rhodamine-labeled phalloidin and the nuclei were stained with 4,6-diamidino-2-phenylindole (DAPI) according to a previously reported protocol.[35] The stained cells were visualized by fluorescence microscopy. The number of DAPI-positive nuclei was calculated in at least 10 fields of view at 100× and 400× magnification and then represented as the number of cells per 1 mm^2. The morphology of the individual cells and their colonies was assessed by staining the cytoskeletal structure. All the biological tests were run in triplicate. Statistical analysis was performed using GraphPad Prism software. All the results were presented as the mean ± standard deviation. Statistical significance was evaluated using the Mann–Whitney *U*-test; a value of $p < 0.05$ was considered significant.

Results and discussion

Synthesis and characterization of M-ALGs

Photo-crosslinking, alike the over other chemical crosslinking methods, allows the fiber scaffold to be crosslinked without destroying the fiber structure, which can happen when fibers are immersed in a solvent medium with a crosslinking agent. It also provides better stability compared to ionic crosslinking because ions can be leached out in physiological media. We used the reaction with GM as the most straightforward way to introduce a photo-crosslinkable group. The outcome of the reaction of ALG with GM significantly depends on the pH of the reaction mixture, *i.e.*, an epoxide ring-opening mechanism (the upper reaction route shown in Scheme 1) is predominant at acidic pH, while a transesterification mechanism (the lower reaction route shown in Scheme 1) is predominant at a basic pH of approximately 10.[36] Therefore, we kept the pH of the reaction

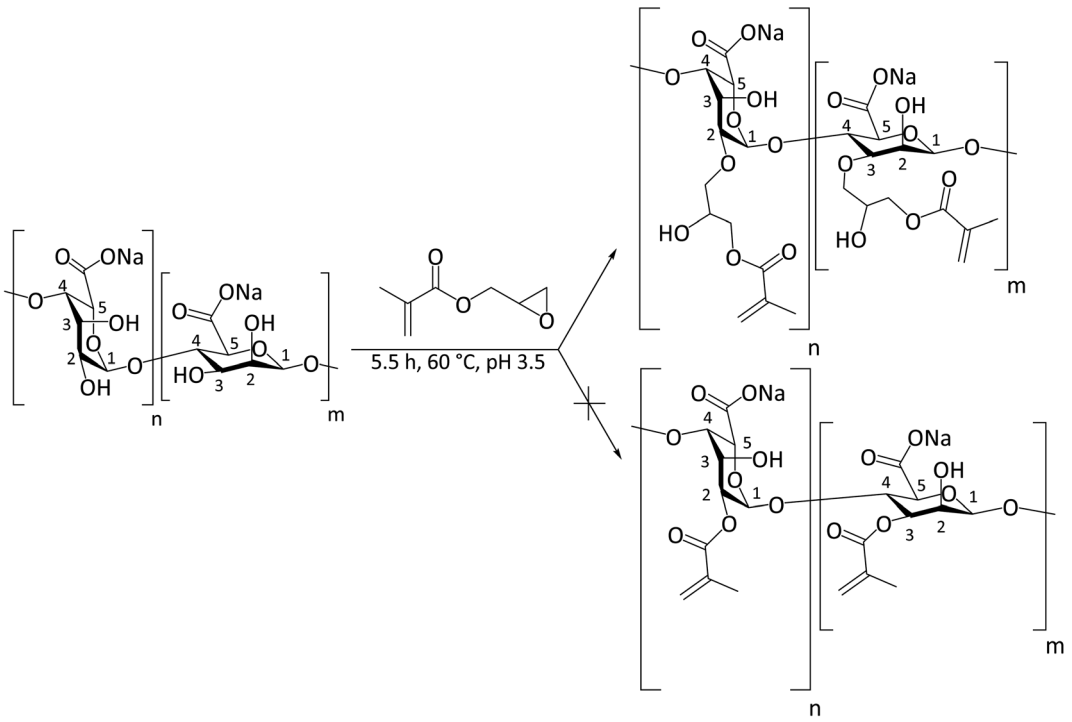

Scheme 1 Synthesis of M-ALG.

mixture at pH 3.5 during whole reaction time by adding acetic acid to ensure the epoxide ring-opening mechanism.[37]

The starting ALG (DS = 0) and the obtained M-ALGs (DS = 0.30 and 0.55) were characterized by ^{1}H NMR spectroscopy (Fig. 1). The broad signals in the range of 4.0–4.6 ppm corresponded to the H2, 3, 4, and 6 protons of the ALG backbone.[13] The signals at 5.6 ppm (signals A in Fig. 1), 5.2 ppm (signals B), and 4.9 ppm (signals C) corresponded to the H1 and H5 of the G unit and M unit depending on the environment.[32] According to the American Society for Testing and Materials (ASTM) international F2259 standard test method for determining the chemical composition and sequence in ALG by ^{1}H NMR spectroscopy, signal A represents H1G, while signal B is divided into four signals corresponding to H5G and H1M. Signal C represents the remaining H5G positions. Therefore, B + C accumulate all positions of H5G and H1M protons and can be used as a reference to calculate F_G[31] and DS. The F_G of the starting ALG was calculated to be 0.5. The M/G ratio is important for biomedical applications[38] because the M/G ratio affects the gelling properties of ALG. The higher the M/G ratio, the more elastic and soft the gel becomes.[39] It also affects the electrospinnability because the repeating of the G units forms strong H-bonds and prevents the molecular entanglement favorable for electrospinning.[40] The signals around 6.6 ppm (signals D) and 6.2 ppm (signals E) corresponded to the vinyl protons of the substituent and the signals around 2.4 ppm corresponded to the methyl protons of the substituent.[13] The DS increased from 0.30 to 0.55 when the reaction time was increased from 4 h to 5.5 h.

The modification of ALG was also confirmed by its ^{13}C NMR spectrum (Fig. 2). The signals in the range of 60–80 ppm represented the ALG backbone carbon atoms, while the one at 100 ppm corresponded to the anomeric carbon atoms. The signal at 169 ppm corresponded to the carbon atom of uronic acid. The two signals at 135 and 127 ppm corresponded to the carbon atoms of the vinyl group and the signals at 17 ppm corresponded to the carbon atoms of the methyl group.

The FTIR spectra of the starting ALG (DS = 0) and the obtained M-ALGs (DS = 0.30 and 0.55) are shown in Fig. 3. Two broad absorption bands at 3700–3000 and 3000–2800 cm^{-1} that corresponded respectively to the stretching vibration of –OH and –CH groups were identically observed for all the samples.[13] Adsorption bands in the range of 1800–800 cm^{-1} were also specific for ALG; including peaks at 1600 cm^{-1} (COO– asymmetric stretching), 1404 cm^{-1} (C–OH deformation and COO– symmetric stretching), 1085 and 1025 cm^{-1} (C–O stretching of pyranose ring), 949 cm^{-1} (C–O stretching in uronic acid residue), and 885 and 813 cm^{-1} (C–H deformation in β-mannuronic acid residue for anomeric and non-anomeric protons, respectively). The spectra of M-ALGs showed stronger absorptions in the 3000–2800 cm^{-1} region compared to the starting unmodified ALG. Furthermore, there were new absorption bands at 1705 cm^{-1} with a shoulder at 1744 cm^{-1}. The former corresponded to the stretching vibration of –CH and the latter to that of the C=O groups in the introduced methacrylate moieties.[13] In addition, absorption bands were also observed at 1295 and 1165 cm^{-1} that could be attributed to the C–O–C stretching vibrations of the substituent. The intensities of these bands increased with increasing the DS. In general, the presence of the vinyl group can be detected by C=C stretching at 1640 cm^{-1} and double bond = C–H bending at 950 cm^{-1}.[41] However, these bands overlapped with the ALG bands in the spectra of the M-ALGs.

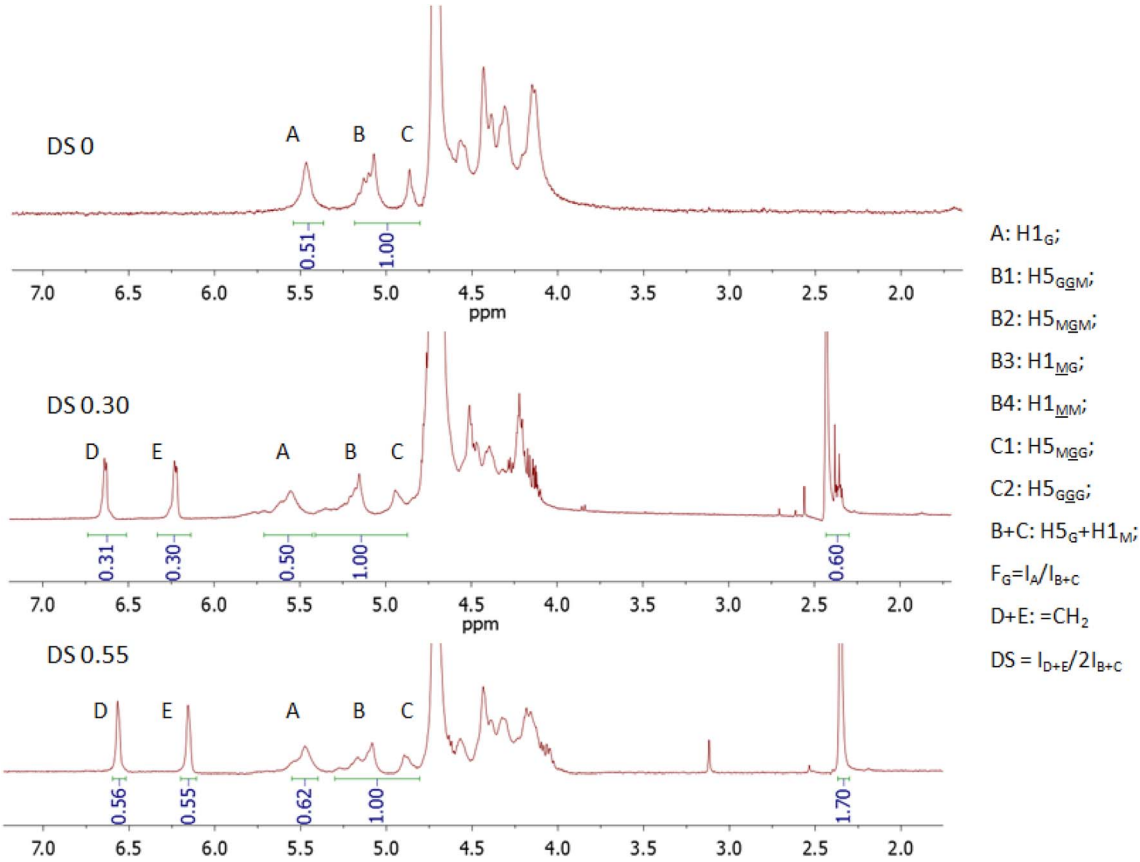

Fig. 1 ^{1}H NMR spectra of ALG and M-ALGs.

Spinning solution property

Prior to the electrospinning of M-ALGs, aqueous solutions of unmodified ALG, PEO as the carrier polymer, and Triton X-100 as the surfactant were prepared and their solution properties, such as viscosity, conductivity, and surface tension, were investigated. To assess the impact of the main solution components on the spinning solution properties, a full factorial design analysis[42] was employed to the solution components (ALG, PEO, and surfactant Triton X-100) and the solution parameters (viscosity, surface tension, and conductivity), as listed in Table 1. The viscosity of the solution significantly varied from 18 142 mPa s (entry 1) to 458 mPa s (entry 8) with the varying concentration of the solution components. Normalized coefficients of 2^3 factorial design were estimated from the model in eqn (1) according to eqn (2), where x is the experimental factor, y is the response, b_0 is the average experimental response, coefficients b_i are the estimated effects of the factors, b_{ij} is the interaction terms, N is number of experiments, and i is the number of factors.

$$y = b_0 + b_1x_1 + b_2x_2 + b_3x_3 + b_{12}x_{12} + b_{13}x_{13} + b_{23}x_{23} \quad (1)$$

$$b_i = \frac{1}{N}\sum_{u=1}^{N} x_u y_u \quad (2)$$

Normalized coefficients for the relationship between the concentrations of the solution components and the viscosity showed that the concentration of ALG had a greater effect on the viscosity than that of PEO (Fig. 4). Furthermore, the combined effects of two and three of the polymers on the viscosity was observed. This interaction may be critical in the PEO-assisted electrospinning of ALG. Increasing the concentration of Triton X-100 slightly affected the surface tension of the solution. The conductivity (2.4 ± 0.1 mS cm^{-1} in all the cases) was not affected by the composition of the solution.

Preparation of the M-ALG fiber mats

Both the needle (capillary) and the needleless electrospinning techniques were employed for preparation of the M-ALG (DS = 0.55) fiber mats. The electrospinning parameters were first studied using unmodified ALG, and then the optimized conditions were applied for M-ALG. At first, the needle electrospinning of ALG with PEO was investigated (Fig. 5). The concentrations of ALG (0–5%) and PEO (0–4%) were varied with each other to optimize the total polymer concentration and the ratio of PEO to ALG through analysis of the electrospun products by optical microscopy. Previously, it was reported that the addition of surfactants facilitates the electrospinning of ALG aqueous solutions by decreasing their surface tensions.[22] Therefore, we added Triton X-100 (0.5–1%) as a surfactant in the spinning solutions. When the concentration of PEO was below

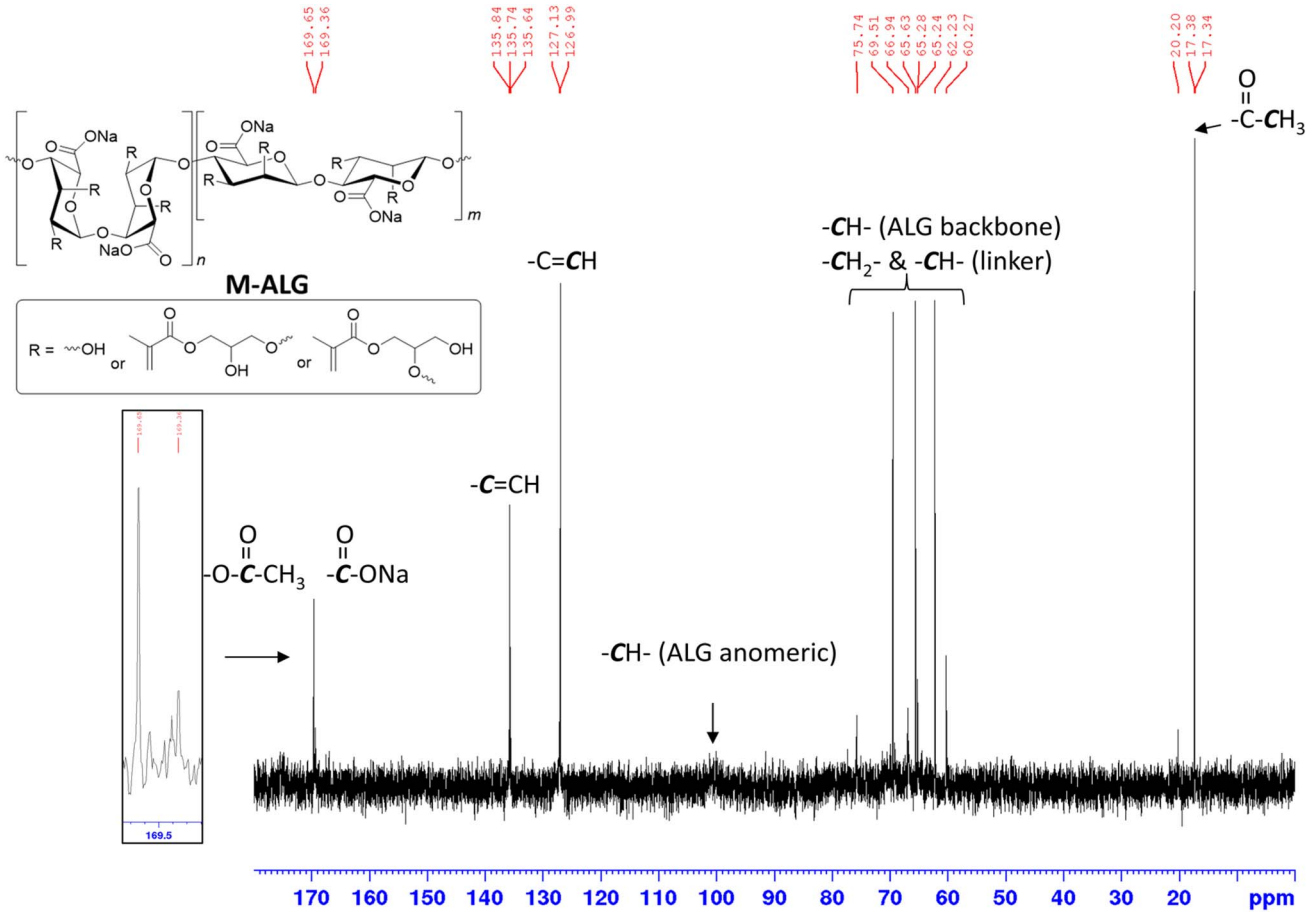

Fig. 2 ^{13}C NMR spectrum of M-ALG (DS = 0.55) in D_2O at 25 °C.

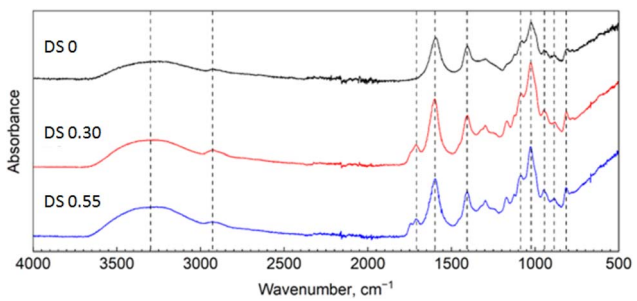

Fig. 3 FTIR spectra of the ALG and M-ALG samples.

Table 1 Spinning solution compositions and their properties in a full factorial model

Entry	[ALG] (%)	[PEO] (%)	[Triton] (%)	Viscosity (Pa s)	Surface tension (mN m^{-1})
1	4	4	1	18	28.7 ± 0.2
2	4	4	0.1	13	31.7 ± 0.4
3	4	1	1	2.1	32.4 ± 0.2
4	4	1	0.1	2.1	32.6 ± 0.3
5	2	4	1	2.3	33.3 ± 0.3
6	2	4	0.1	2.3	32.2 ± 0.2
7	2	1	1	0.43	28.8 ± 0.1
8	2	1	0.1	0.46	30.5 ± 0.5

2%, the polymer mixture formed particles or beaded fibers (when ALG was 5% and PEO was 2%) *via* the electrospray process due to the low viscosity (see Table 1 entries 3, 4, 7, and 8). Increasing the concentration of PEO above 3% allowed forming uniform bead-free fibers thanks to the higher viscosity (see Table 1 entries 1, 2, 5, and 6). Hence, it was found that the total polymer concentration of 6–8% with a PEO to ALG ratio from 0.6 to 1 gave nice fibers. Another indicative parameter for needle electrospinning is the flow rate. In general, by increasing the polymer concentration, the viscosity increases and the optimal flow rate decreases. Herein, the flow rate was varied from 2 to 30 μL min^{-1} depending on the concentration. Consequently, the optimal conditions for the needle electrospinning of "non-functionalized" ALG (4%), PEO (4%), and Triton X-100 (0.5%) was determined as follows: voltage of 30 kV, flow rate of 15 μL min^{-1}, distance between electrodes of 15 cm, and needle gauge of 18 GA. For the electrospinning of M-ALG, the photoinitiator I2959 (0.3% w/v, *i.e.*, 7.5% compared to the M-ALG) was added into the mixture of M-ALG (4%), PEO (4%), and Triton X-100 (0.5%). The concentration of the photoinitiator was determined as the minimum amount required for

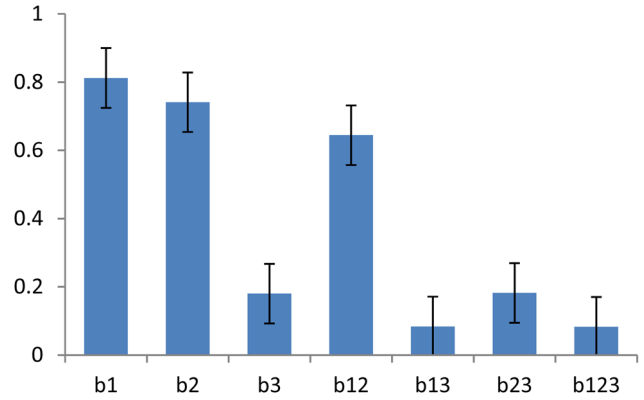

Fig. 4 Normalized coefficients of 2^3 factorial design for the relationship between the concentrations of the solution components (b1: ALG concentration, b2: PEO concentration, b3: Triton X-100 concentration) and viscosity.

effective crosslinking by taking into account the potential toxicity. The same electrospinning condition as for ALG was applied except for the flow rate, which was decreased to 2 μL min^{-1} due to the higher viscosity of M-ALG than ALG.

The needleless electrospinning process was also optimized in a similar way. The greatest difference in the needleless electrospinning from the needle approach is its very high applicable voltage (~65 kV), which enables an about 1.5 times higher electric field than in the capillary process. Thanks to the high applied voltage, we could reduce the minimum concentration of PEO to 0.6%, corresponding to a PEO to ALG ratio of 0.2. Furthermore, it enabled forming smooth uniform fibers without needing to add a surfactant to the spinning solution. Consequently, the optimized parameters for the needleless electrospinning of M-ALG (4%), PEO (0.8%), and I2959 (0.3%) were determined as follows: voltage of 60 kV, distance between electrodes of 22 cm, and the spinning electrode rotation speed of 8 rpm.

According to Saquing *et al.*,[43] carrier polymers such as PEO and PVA favorably reduce the electrical conductivity and surface tension of the solutions. Furthermore, they provide molecular entanglement and "carry" ALG from the solution to fibers during electrospinning. In their report, the authors achieved 70% ALG content in the fibers using PEO with a high molecular weight (2×10^6 Da), and 85% ALG content by adding Triton X-100 surfactant *via* the needle electrospinning process. In our case, the needleless electrospinning process allowed increasing the ALG content in the fibers to 80% (using PEO of 4×10^5 Da as the carrier polymer) without needing the addition of a surfactant. Decreasing the PEO content can positively affect the photo-crosslinking process, as PEO interferes in the contacts between photo-crosslinkable groups.

To ensure the photo-crosslinking ability of M-ALG, we first applied UV irradiation to the aqueous solutions of M-ALG containing the photoinitiator I2959. After 30 min irradiation, the solutions were converted into hydrogels, which indicated the photo-crosslinking had successfully occurred. Hence, the electrospun fiber mats were also irradiated with UV under the same condition. After the irradiation, the fiber mats became insoluble in water for one month, while the fiber mats before irradiation were completely soluble in water. The photo-crosslinked fiber mats were exposed to water for 24 h to wash out PEO used as the carrier polymer from the insoluble crosslinked fiber mats.

Physical property of the fiber mats

The morphology of the electrospun M-ALG fiber mats was characterized by SEM and AFM (Fig. 6). The fiber mats of M-ALG (DS = 0.55) prepared by the needle- and the needleless electrospinning had average fiber diameters of 148 ± 22 and 164 ± 17 nm, and average pore sizes of 0.54 ± 0.24 and 0.27 ± 0.15 μm^2, respectively. This suggests that the needleless electrospinning could provide more densely packed fibers in the mat. The surface roughness of the fiber mat was roughly estimated

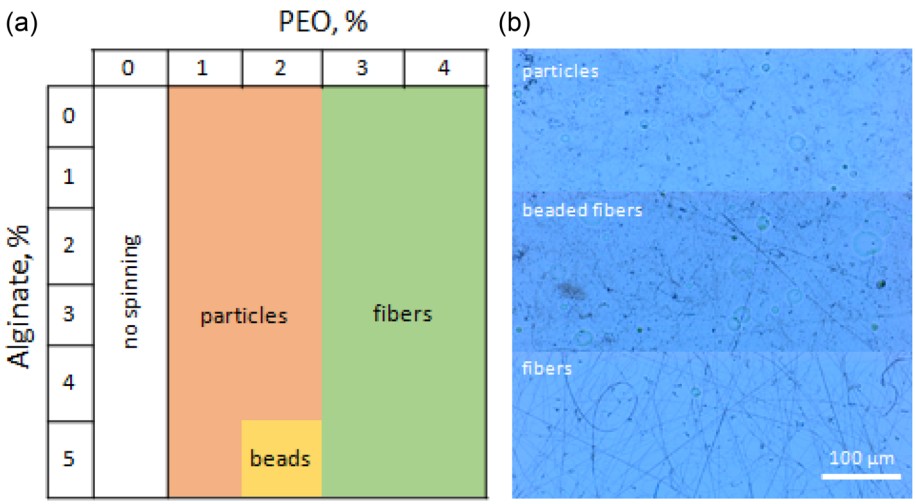

Fig. 5 (a) Phase diagram of the needle electrospun products from the mixture of ALG, PEO, and Triton X-100 with different concentrations and (b) optical microscopy images of the electrospun products.

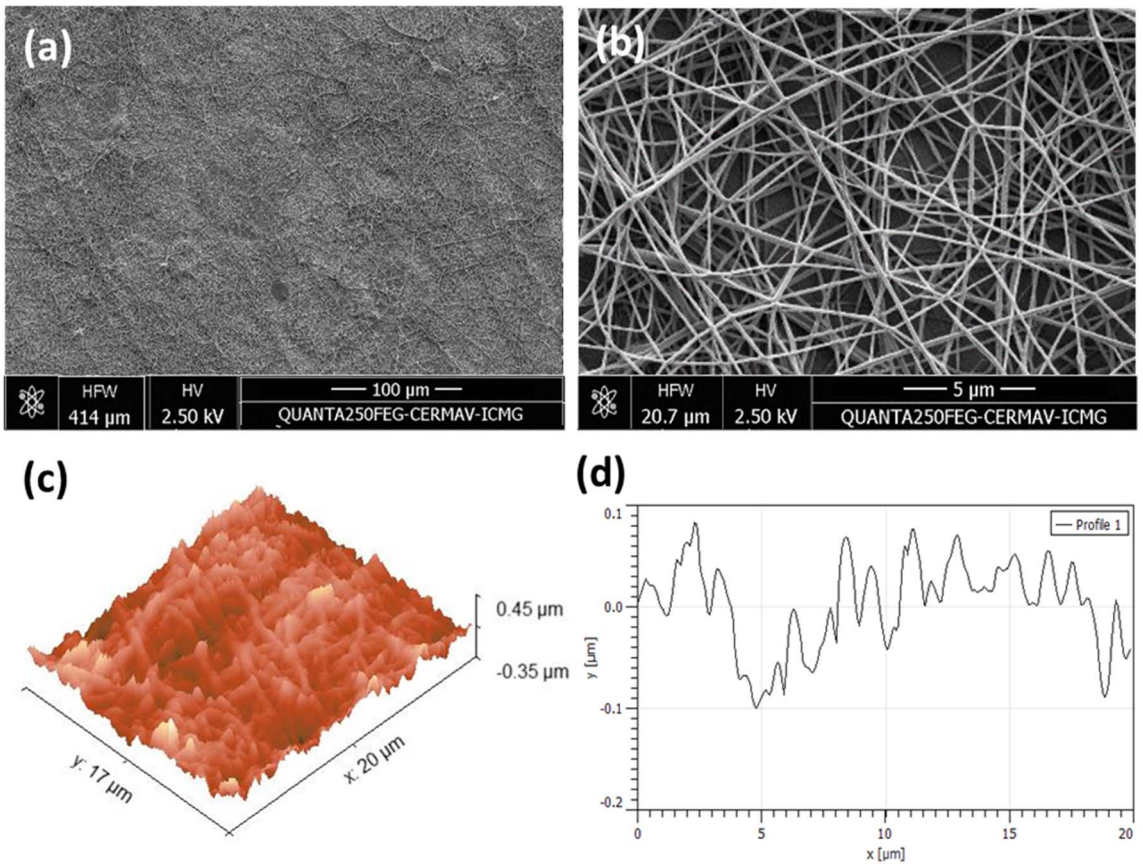

Fig. 6 (a) Broad and (b) enlarged SEM images, AFM (c) 3D topographical image and (d) 2D surface roughness profile of the needle electrospun M-ALG fiber mat (DS 0.55).

as 0.1 µm, which is commonly observed for electrospun fiber mats,[34] from the AFM topological images shown in Fig. 6c and d.

The mechanical properties of the unmodified ALG and the M-ALG fiber mats were investigated by tensile test before and after UV irradiation, and the obtained Young's modulus (E), tensile strength (σ_y), breaking stress (σ_b), and elongation at break (ε_b) are summarized in Table 2. The introduction of methacrylate groups into ALG resulted in a 2-fold decrease in Young's modulus of the M-ALG fiber mat ($E = 109 \pm 8$ MPa) in comparison to the ALG fiber mat ($E = 214 \pm 18$ MPa), as listed in entries 1 and 3. Accordingly, the tensile strength of the M-ALG fiber mat ($\sigma_y = 5.3 \pm 0.1$ MPa) was also decreased in comparison to the ALG fiber mat ($\sigma_y = 3.5 \pm 0.1$ MPa). It can be argued that the introduction of methacrylate groups into the ALG backbone resulted in a decrease in the total energy of interchain interactions in the material, *i.e.*, the methacrylate groups played a role of internal plasticizer. It should be noted that this difference in stiffness (Young's modulus) was observed for both the original and the UV-irradiated fiber mats. However, the difference in Young's modulus between the ALG fiber mat ($E = 249 \pm 12$ MPa) and the M-ALG fiber mat ($E = 149 \pm 6$ MPa) after UV irradiation (entries 2 and 4) was slightly smaller than for the non-irradiated samples (entries 1 and 3). Apparently, the new interchain crosslinks formed during the UV irradiation partially compensated for the plasticizing effect of the methacrylate groups. Such effects were observed as the difference in the values of elongation at break (ε_b), *i.e.*, the ALG fiber mats had 1.6 (before UV) to 1.9 (after UV) times smaller ε_b values than the M-ALG fiber mats. The UV irradiation to the fiber mats increased their Young's moduli, while values of elongation at break values only slightly decreased. The introduction of a substituent may also disrupt the hydrogen bonding interactions between nearby macromolecules, contributing to a decrease in strength.

Table 2 Mechanical characteristics of the ALG-based electrospun scaffolds

Entry	Fiber mats	E (MPa)	σ_y (MPa)	σ_b (MPa)	ε_b (%)
1	ALG	214 ± 18	5.3 ± 0.1	7.4 ± 0.4	9.5 ± 0.9
2	ALG after UV	249 ± 12	6.2 ± 0.3	8.1 ± 0.7	8.5 ± 0.7
3	M-ALG	109 ± 8	3.5 ± 0.1	7.1 ± 0.2	18 ± 1
4	M-ALG after UV	149 ± 6	4.2 ± 0.1	6.5 ± 0.8	14 ± 1

MSCs cultivation on the M-ALG and CS fiber mat scaffolds

The photo-crosslinked M-ALG fiber mat was used as a scaffold for MSCs cultivation in α-MEM medium. Here, an electrospun CS fiber mat was used as a comparison because CS provides sufficient cell adhesion either through its positive charge[44] or by

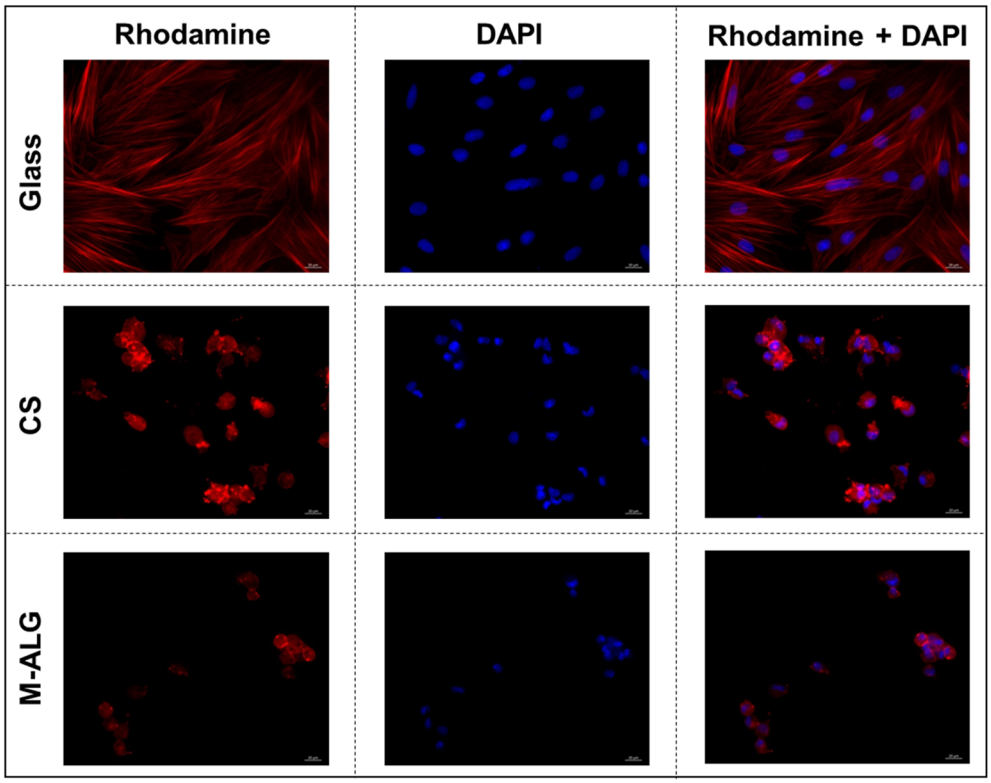

Fig. 7 Fluorescent microscopic images (400× magnification) of MSCs adhered on the surface of the scaffolds (glass: top, CS fiber mat: middle, and M-ALG fiber mat: bottom) with a stained cytoskeleton (Rhodamine: left), nuclei (DAPI: center), and merged images (Rhodamine + DAPI: right).

possible interaction with the cell binding and regulatory receptors[45] due to its structural similarity to hyaluronic acid, one of the major components of the ECM. A potential drawback of CS is its very strong interaction with cells, which may interfere with migrations of the cells. The cultivated MSCs on glass and the M-ALG and CS fiber mats were stained with rhodamine-labeled phalloidin (to visualize the cytoskeleton) and DAPI (to visualize the nuclei),[35] and then observed by fluorescent microscopy (Fig. 7). On the glass, the MSCs formed a uniform syncytium-like confluent monolayer, *i.e.*, the cells were elongated with pseudopodia and some of them had signs of proliferation. Red-stained actin filaments were clearly elongated and linear. The cell adhesion property of the M-ALG fiber mat was weaker than that of the CS fiber mat, as suggested by the lower number of nuclei on the M-ALG fiber mat ($72 \pm 15/mm^2$) than on the CS fiber mat ($206 \pm 40/mm^2$), as listed in Table 3. In contrast, multiple round cells arranged separately and in small colonies with diffusely stained cytoplasm were observed on the electrospun M-ALG and CS fiber mats. The cell colonies consisted of a small number of cells, and had a spheroid-like shape, without signs of cell migration. It should be noted that such spherical-shaped colonies formed by adhered cells have been commonly observed on electrospun fibrous scaffolds, as well as for materials based on CS or hyaluronic acid.[3,34,46] In addition to sufficient colony growth, the presence of a large number of individually located round cells (probably apoptotic) and the absence of signs of cell migration along the periphery of the colonies indicated the suboptimal conditions for cell adhesion and proliferation and the need for further increasing the biocompatible properties of the electrospun M-ALG scaffold. On the other hand, the MSCs formed colonies on the M-ALG fiber mat with a similar morphology and size (28 ± 4 μm) compared to those on the CS fiber mat (31 ± 7 μm). This indicates the cytocompatibility of the M-ALG fiber mat despite the presence of the photoinitiator, which is consistent with previous studies on photo-crosslinked ALG hydrogels.[15]

Table 3 Number of adherent MSCs and maximum sizes of spherical cell colonies

Sample	Cell morphology	Adhered cells (number/mm^2)	Mean diameter of the colonies (μm)
Glass	Multiple elongated cells, flat colonies, monolayer	—	—
CS fiber mat	Single elongated and multiple round cells, spheroids	206 ± 40	31 ± 7
M-ALG fiber mat		72 ± 15	28 ± 4

Conclusions

In summary, we here proposed a new cytocompatible scaffold for MSCs cultivation prepared by electrospinning of the photo-crosslinkable M-ALG with PEO as the carrier polymer, followed by the photo-crosslinking and the elimination of PEO by washing with water. Both the needle and needleless electrospinning techniques were applicable for the productions. In particular, the needleless technique enabled reducing the concentration of PEO and eliminated the need to use a surfactant thanks to its high applicable voltage (~65 kV). The M-ALG fiber mat showed similar cytocompatibility to MSCs as the electrospun CS fiber mat, while its cell adhesion property was relatively weaker than that of the CS fiber mat. The presence of the photoinitiator did not significantly decrease the cytocompatibility of M-ALG mat. Although the results suggested limited cell migration and suboptimal conditions for cell adhesion and proliferation for M-ALG, these issues could be further addressed with the present method. Electrospinning followed by photo-crosslinking can incorporate different water-soluble polysaccharides to adjust the adhesive properties; it is also possible to use low molecular weight alginate to ensure its better biodegradability. Our results suggest the potential application of M-ALG electrospun fiber mats as scaffolds for tissue engineering.

Data availability

All of the data generated in this study are present in the manuscript.

Conflicts of interest

There are no conflicts to declare.

Acknowledgements

The authors acknowledge Dr C. Lancelon-Pin for the SEM observation at the Electronic Microscopy Platform (PMIEL) of the Institut de Chimie Moléculaire de Grenoble (ICMG). I.O. thanks the Centre de Recherches sur les Macromolécules Végétales (CERMAV, CNRS) for their financial supports. D.P. and Y.S. thank the National Research Center Kurchatov Institute for the financial support of this research, which was conducted under the Government Contract No.124013000730-3.

References

1 A. D. Theocharis, S. S. Skandalis, C. Gialeli and N. K. Karamanos, *Adv. Drug Delivery Rev.*, 2016, **97**, 4–27.
2 D. Poshina and I. Otsuka, *Textiles*, 2021, **1**, 152–169.
3 V. A. Petrova, A. S. Golovkin, A. I. Mishanin, D. P. Romanov, D. D. Chernyakov, D. N. Poshina and Y. A. Skorik, *Biomedicines*, 2020, **8**, 305.
4 R. Abka-Khajouei, L. Tounsi, N. Shahabi, A. K. Patel, S. Abdelkafi and P. Michaud, *Mar. Drugs*, 2022, **20**, 364.
5 R. Gheorghita Puscaselu, A. Lobiuc, M. Dimian and M. Covasa, *Polymers*, 2020, **12**, 2417.
6 D. R. Sahoo and T. Biswal, *SN Appl. Sci.*, 2021, **3**, 30.
7 E. Ruvinov and S. Cohen, *Adv. Drug Delivery Rev.*, 2016, **96**, 54–76.
8 K. H. Bouhadir, K. Y. Lee, E. Alsberg, K. L. Damm, K. W. Anderson and D. J. Mooney, *Biotechnol. Prog.*, 2001, **17**, 945–950.
9 A. Sood, A. Gupta and G. Agrawal, *Carbohydr. Polym. Technol. Appl.*, 2021, **2**, 100067.
10 S. S. Majidi, P. Slemming-Adamsen, M. Hanif, Z. Zhang, Z. Wang and M. Chen, *Int. J. Biol. Macromol.*, 2018, **118**, 1648–1654.
11 H. Samadian, H. Maleki, Z. Allahyari and M. Jaymand, *Coord. Chem. Rev.*, 2020, **420**, 213432.
12 D. C. Aduba Jr and H. Yang, *Bioengineering*, 2017, **4**, 1.
13 F. Araiza-Verduzco, E. Rodríguez-Velázquez, H. Cruz, I. A. Rivero, D. R. Acosta-Martínez, G. Pina-Luis and M. Alatorre-Meda, *Materials*, 2020, **13**, 534.
14 X. Wang, T. Hao, J. Qu, C. Wang and H. Chen, *J. Nanomater.*, 2015, **2015**, 970619.
15 O. Jeon, K. H. Bouhadir, J. M. Mansour and E. Alsberg, *Biomaterials*, 2009, **30**, 2724–2734.
16 A. D. Rouillard, C. M. Berglund, J. Y. Lee, W. J. Polacheck, Y. Tsui, L. J. Bonassar and B. J. Kirby, *Tissue Eng., Part C*, 2011, **17**, 173–179.
17 M. D. Brigham, A. Bick, E. Lo, A. Bendali, J. A. Burdick and A. Khademhosseini, *Tissue Eng., Part A*, 2009, **15**, 1645–1653.
18 M. M. Stevens, *Biophys. J.*, 2011, **100**, 189a.
19 J. Pelipenko, P. Kocbek and J. Kristl, *Int. J. Pharm.*, 2015, **484**, 57–74.
20 K. Y. Lee, L. Jeong, Y. O. Kang, S. J. Lee and W. H. Park, *Adv. Drug Delivery Rev.*, 2009, **61**, 1020–1032.
21 D. Poshina, I. Tyshkunova, V. Petrova and Y. A. Skorik, *Rev. Adv. Chem.*, 2021, **11**, 112–133.
22 J. Wróblewska-Krepsztul, T. Rydzkowski, I. Michalska-Pożoga and V. K. Thakur, *Nanomaterials*, 2019, **9**, 404.
23 G. Huerta-Angeles, M. Brandejsová, K. Knotková, M. Hermannová, M. Moravcová, D. Šmejkalová and V. Velebný, *Carbohydr. Polym.*, 2016, **137**, 255–263.
24 X. Chen, B. Lu, D. Zhou, M. Shao, W. Xu and Y. Zhou, *Int. J. Biol. Macromol.*, 2020, **155**, 903–910.
25 K. C. de Castro, J. Burga-Sánchez, M. G. N. Campos and L. H. I. Mei, *RSC Adv.*, 2020, **10**, 31271–31279.
26 Y. Zhou, Q. Dong, H. Yang, X. Liu, X. Yin, Y. Tao, Z. Bai and W. Xu, *Carbohydr. Polym.*, 2017, **168**, 220–226.
27 Y. Zhou, K. Liang, C. Zhang, J. Li, H. Yang, X. Liu, X. Yin, D. Chen, W. Xu and P. Xiao, *Cellulose*, 2017, **24**, 4253–4262.
28 P. Alves, M. Santos, S. Mendes, S. P. Miguel, K. D. de Sá, C. SD Cabral, I. J. Correia and P. Ferreira, *Polymers*, 2019, **11**, 653.
29 X. Yang, D. Yang, X. Zhu, J. Nie and G. Ma, *Eur. Polym. J.*, 2019, **113**, 142–147.
30 S. I. Jeong, O. Jeon, M. D. Krebs, M. C. Hill and E. Alsberg, *Eur. Cells Mater.*, 2012, **24**, 331.
31 M. Davidovich-Pinhas and H. Bianco-Peled, *Carbohydr. Polym.*, 2010, **79**, 1020–1027.
32 H. Grasdalen, B. Larsen and O. Smidsrød, *Carbohydr. Res.*, 1979, **68**, 23–31.

33 A. A. Karpov, Y. K. Uspenskaya, S. M. Minasian, M. V. Puzanov, R. I. Dmitrieva, A. A. Bilibina, S. V. Anisimov and M. M. Galagudza, *Int. J. Exp. Pathol.*, 2013, **94**, 169–177.
34 V. A. Petrova, D. D. Chernyakov, D. N. Poshina, I. V. Gofman, D. P. Romanov, A. I. Mishanin, A. S. Golovkin and Y. A. Skorik, *Materials*, 2019, **12**, 2016.
35 E. Bolbasov, S. Goreninskii, S. Tverdokhlebov, A. Mishanin, A. Viknianshchuk, D. Bezuidenhout and A. Golovkin, *IOP Conf. Ser.:Mater. Sci. Eng.*, 2018, **350**, 012012.
36 A. V. Reis, A. R. Fajardo, I. T. Schuquel, M. R. Guilherme, G. J. Vidotti, A. F. Rubira and E. C. Muniz, *J. Inorg. Biochem.*, 2009, **74**, 3750–3757.
37 M. Hasany, S. Talebian, S. Sadat, N. Ranjbar, M. Mehrali, G. G. Wallace and M. Mehrali, *Appl. Mater. Today*, 2021, **24**, 101150.
38 Z. Belattmania, S. Kaidi, S. El Atouani, C. Katif, F. Bentiss, C. Jama, A. Reani, B. Sabour and V. Vasconcelos, *Molecules*, 2020, **25**, 4335.
39 J. I. Murillo-Álvarez and G. Hernández-Carmona, *J. Appl. Phycol.*, 2007, **19**, 545–548.
40 H. Nie, A. He, J. Zheng, S. Xu, J. Li and C. C. Han, *Biomacromolecules*, 2008, **9**, 1362–1365.
41 S. A. Baghban, M. Ebrahimi, S. Bagheri-Khoulenjani and M. Khorasani, *RSC Adv.*, 2021, **11**, 14996–15009.
42 G. E. P. Box, J. S. Hunter and W. G. Hunter, *Statistics for Experimenters: Design, Innovation, and Discovery*, Wiley, 2005.
43 C. D. Saquing, C. Tang, B. Monian, C. A. Bonino, J. L. Manasco, E. Alsberg and S. A. Khan, *Ind. Eng. Chem. Res.*, 2013, **52**, 8692–8704.
44 N. Aibani, R. Rai, P. Patel, G. Cuddihy and E. K. Wasan, *Pharmaceutics*, 2021, **13**, 1686.
45 W. Rao, H. Wang, J. Han, S. Zhao, J. Dumbleton, P. Agarwal, W. Zhang, G. Zhao, J. Yu and D. L. Zynger, *ACS Nano*, 2015, **9**, 5725–5740.
46 T. C. Tseng, C. W. Wong, F. Y. Hsieh and S. h. Hsu, *Biotechnol. J.*, 2017, **12**, 1700064.